
# Data Analyses from Seismic Instrumentation Installed on the I-40 Bridge

## Determination of When Crack Occurred on the Hernando de Soto I-40 Bridge

Research Final Report from the University of Memphis | Shahram Pezeshk, Charles Camp, Ali Kashani, and Mohsen Akhani| October 31, 2021

Sponsored by Tennessee Department of Transportation Long Range Planning Research Office & Federal Highway Administration

THE UNIVERSITY OF MEMPHIS

# DISCLAIMER

This research was funded through the State Planning and Research (SPR) Program by the Tennessee Department of Transportation and the Federal Highway Administration under ***A Task to Perform Data Analyses from Seismic Instrumentation Installed on the I-40 Bridge.***

# Technical Report Documentation Page

| 1. Report No. | 2. Government Accession No. | 3. Recipient's Catalog No. |
|---|---|---|
| 4. Title and Subtitle<br>*Data Analyses from Seismic Instrumentation Installed on the I-40 Bridg* | | 5. Report Date<br>October 31, 2021<br>6. Performing Organization Code |
| 7. Author(s)<br>Shahram Pezeshk, Charles V. Camp, Ali Kashani, and Mohsen Akhani | | 8. Performing Organization Report No. |
| 9. Performing Organization Name and Address<br>Department of Civil Engineering<br>The University of Memphis<br>Memphis, TN 38152 | | 10. Work Unit No. (TRAIS)<br>11. Contract or Grant No. |
| 12. Sponsoring Agency Name and Address<br>Tennessee Department of Transportation<br>505 Deaderick Street, Suite 900<br>Nashville, TN 37243 | | 13. Type of Report and Period Covered<br>Final Report<br>06/01/2021 to 10/31/2021<br>14. Sponsoring Agency Code |

15. Supplementary Notes
Conducted in cooperation with the U.S. Department of Transportation, Federal Highway Administration.

16. Abstract

The Hernando De Soto I-40 Bridge spans over the Mississippi River connecting Tennessee and Arkansas. On May 11, 2021, this bridge was closed after detecting a fraction in one of the major 900-ft horizontal tension tie girders. Inspections conducted by officials from both the Tennes-see and Arkansas departments of transportation revealed that the crack was there for many years. Despite much debate and many investigations, determining the time when the crack first formed is challenging. However, it is important to answer this question because, in bridges de-signs like the I-40 Bridge, a crack in or the failure of critical elements might result in the collapse of the whole structure. Therefore, determining the time when the crack first affects the perfor-mance of the bridge and reviewing the actions within this period can be helpful to update and modify the strategies and regulations for health monitoring these structures.

The purpose of this research was to determine the time when the crack occurred using the am-bient vibration data collected by the seismic instrumentation installed on the bridge. A network of sensors on the I-40 Bridge installed and maintained by the University of Memphis was used to determine when the cracked element first affected the behavior of the bridge. Vibration data recorded on the bridge in 2016, 2017, 2018, 2019, 2020, and 2021 were used in this study. We considered the frequency content of the bridge as one of the unique characteristics of the structures extractable from the recorded data that would change due to damage in the struc-ture. A series of correlation tables were developed by processing and correcting data recorded on the bridge from 2016 to 2021. The results indicate that the tension tie girder crack was first detected in the 2018 data and continued to be developed in 2019 and 2020.

| 17. Key Words | 18. Distribution Statement |
|---|---|
| **Bridge Crack, I-40 Bridge, Seismic Instrumentation, Signal Processing** | No restriction. This document is available to the public from the sponsoring agency at the website http://www.tn.gov/ |

| 19. Security Classif. (of this report) | 20. Security Classif. (of this page) | 21. No. of Pages | 22. Price |
|---|---|---|---|
| Unclassified | Unclassified | 37 | |

## Acknowledgements

The authors would like to thank Mr. Ted Kniazewycz and Ms. Melanie Murphy for their support of this project. The authors would also like to thank Dr. Mehmet Celebi for his suggestions and his guidance. The authors would also like to thank Mr. Steve Brewer for his help sorting and collecting data from the strong-motion instrumentation used in this study.

# Executive Summary

The Hernando de Soto I-40 Bridge spans the Mississippi River connecting Tennessee and Arkansas. On May 11, 2021, this bridge was closed after detecting a fracture in one of the major 900-ft horizontal tension tie girders. Inspections conducted by officials from both the Tennessee and Arkansas departments of transportation revealed that the crack was there for many years. Despite much debate and many investigations, determining the time when the crack first formed is challenging. However, it is important to answer this question because, in bridge designs like the I-40 Bridge, a crack in or the failure of critical elements might result in the collapse of the whole structure. Therefore, determining the time when the crack first affects the performance of the bridge and reviewing the actions within this period can be helpful to update and modify the strategies and regulations for health monitoring these structures.

The purpose of this research was to determine the time when the crack occurred using the ambient vibration data collected by the seismic instrumentation installed on the bridge. A network of sensors on the I-40 Bridge installed and maintained by the University of Memphis was used to determine when the cracked element first affected the behavior of the bridge. Vibration data recorded on the bridge in 2016, 2017, 2018, 2019, 2020, and 2021 were used in this study. We considered the frequency content of the bridge as one of the unique characteristics of the structure extractable from the recorded data that would change due to damage in the structure. A series of correlation tables was developed by processing and correcting data recorded on the bridge from 2016 to 2021. The results indicate that the tension tie girder crack was first detected in the 2018 data and continued to develop in 2019 and 2020.

## *Key Findings*

- By processing and correcting data collected from the I-40 Bridge and developing a series of correlation tables among various recorded data for 2016 to 2021, we can confirm that the tension tie girder crack was initiated in 2018 and developed in 2019 and 2020.

## *Key Recommendations*

- Bridge instrumentation can provide health monitoring of the I-40 Bridge
- Continue to maintain and operate the I-40 Bridge instrumentation

# Table of Contents

# List of Tables

# List of Figures

# Glossary of Key Terms and Acronyms

ARDOT – Arkansas Department of Transportation

TDOT – Tennessee Department of Transportation

CERI – Center for Earthquake Research and Information

FAS – Fourier Amplitude Spectrum

SAC – Seismic Analysis Code

SEED – Standard for the Exchange of Earthquake Data

# Chapter 1 Introduction

The Hernando de Soto I-40 Bridge connecting Memphis, Tennessee, to West Memphis, Arkansas, is a critical structure on a major commercial corridor. The 3.3-mile-long bridge, completed in the early 1970s, carries about 60,000 vehicles daily, according to the Tennessee Department of Transportation (TDOT), which shares responsibility for the bridge with the Arkansas Department of Transportation (ARDOT). The I-40 Bridge carries some of the highest proportions of truck traffic in the country.

> *The purpose of this study is to use the strong-motion instrumentation installed on this bridge by the Department of Civil Engineering and Center for Earthquake Research and Information (CERI) of The University of Memphis to determine the possible time when the crack was initiated.*

A crack in one of two 900-foot horizontal steel tension tie girders critical for the bridge's structural integrity was discovered on May 11, 2021 (see Figure 1-1). Figure 1-2 is a photo from 2019, confirmed by transportation officials to be authentic, that shows the crack was visible in 2019. Another photo appears to show a crack as far back as 2016, but the authenticity of that image remains under investigation. The main span of the I-40 Bridge was shut down abruptly on May 11, 2021, after inspectors called 911 to report the crack. According to ARDOT, the six-lane Hernando de Soto Bridge connecting Tennessee and Arkansas was reopened to eastbound I-40 traffic first and was reopened in both directions on Saturday, July 31, 2021, at 10 PM. The I-40 Bridge reopened following almost three months of emergency repair work. The bridge became a national example of the risks posed by the nation's infrastructure. The emergency repairs on the closed span created major traffic disruptions in the Memphis area while traffic was diverted to the nearby Interstate-55 bridge. Along with the reason behind this fracture, estimating the occurrence time is still an important mystery.

The purpose of this study is to use the strong-motion instrumentation installed on this bridge (Pezeshk et al., 2018) by the Department of Civil Engineering and Center for Earthquake Research and Information (CERI) at The University of Memphis to determine when the tension tie girder crack was initiated.

ARDOT classifies the I-40 Bridge as "fracture critical," meaning parts of the bridge are "subject to tension whose failure would probably cause a portion of or the entire bridge to collapse." Fracture critical bridges require frequent inspections but are not inherently unsafe. That is why detecting a fracture of a primary support beam on the I-40 Bridge led to concerns about a near-collapse of one of the busiest bridges in the United States. Public Information Officer Dave Parker of ARDOT told Talk Business & Politics news that the damaged beam that led to the emergency and immediate closure of the bridge on May 11, 2021, had been sent off for forensic analysis. This fact highlights the requirement for consistent and regular inspections of the bridge. Although a visual inspection is an easy, straightforward, and cost-effective way to identify damage on bridge surfaces, there are many challenges and difficulties associated with this type of monitoring. A visual inspection does not adequately assess the structure's interior or the sections under the bridge, or the overall behavior of the structure. Health monitoring strategies using a variety of instrumentation is a well-established approach to overcome the deficiencies of manual inspections and assure the safety of a structure.

The I-40 Bridge has an intensive strong-motion monitoring system which uses numerous traditional and several non-traditional forms of instrumentation designed to characterize the structure's response to shaking from tectonic and induced sources. The I-40 Bridge has been retrofitted to withstand a magnitude (mb) 7 event at a 65 km distance from the site at a depth of 20 km. The strong-motion seismic instrumentation was designed and installed on the I-40 Bridge by the Department of Civil Engineering and CERI at the University of Memphis. The major purpose of the instrumentation was to examine the performance of the bridge following the retrofit and assess the performance of the base isolation system in the event of an earthquake. Also, the collected data can be used in different ways for various applications. For example, data collected on the behavior of the base isolation system will apply to any structure incorporating this design. Furthermore, lessons learned from the instrumentation of a bridge, like the I-40 Bridge, will provide important and needed information that will apply to structures built on similar seismological and geological settings. Therefore, data collected from the instrumentation of the I-40 Bridge are invaluable assets in evaluating the structure.

In this research project, available data from the I-40 Bridge recorded by the University of Memphis is used to estimate when the tension tie girder crack on the main span beam was initiated. Determining when the crack occurred on the I-40 Bridge would be helpful to understand and determine any deficiencies in the ongoing inspection procedures and provide better guidelines for future activities. Moreover, monitoring the bridge using the installed instrumentation may be considered in future complementary attempts to traditional visual inspections.

While data from the bridge are recorded continuously, only data during an earthquake event are saved. However, data sets from five years (2016, 2017, 2018, 2019, 2020, and 2021) have been downloaded and processed. An analysis of the frequency content of data can show the behavioral signature of the bridge. We believe that a rupture or crack in a bridge element will change the recorded frequency content (a detectable change in the bridge's signature). From analysis and comparison of data collected from various days, months, and years, it was determined that the tension tie girder crack first affected the bridge behavior in 2018. The following sections describe the seismic instrumentation, data processing, and correlations analyses used in this study.

**Figure 1-1. A detected crack in a critical steel support beam of the I-40 Bridge.**

(a)

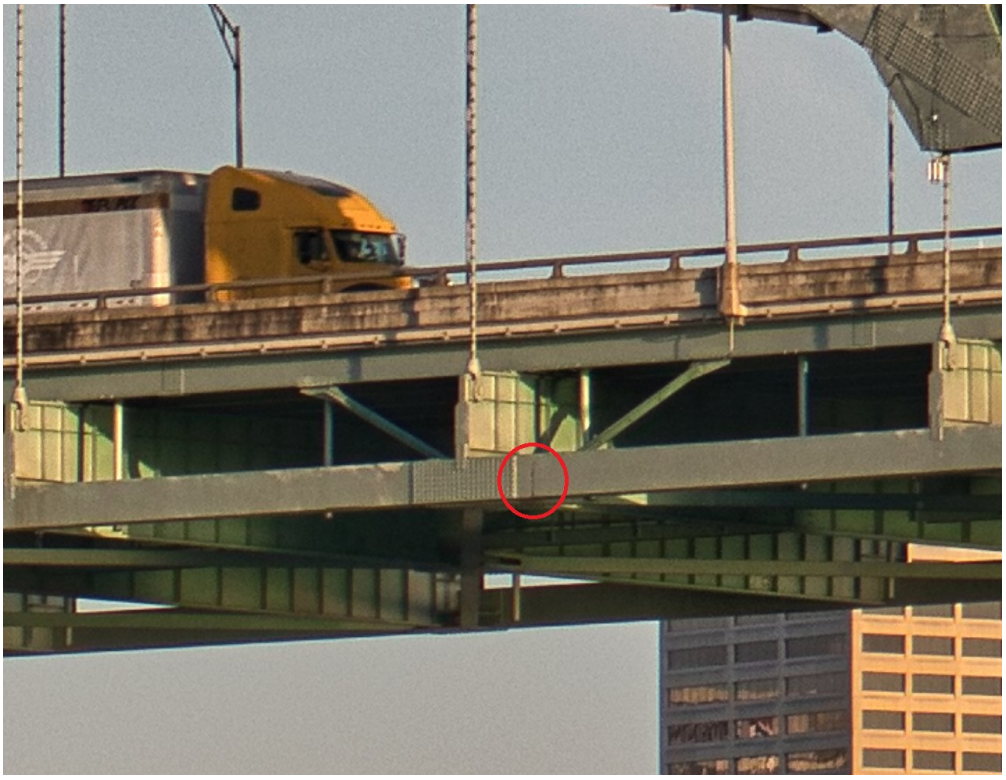

(b)

**Figure 1-2. Photos of the I-40 Bridge in 2019 identifying the crack.**

# Chapter 2 Instrumentation

In 2001, The University of Memphis installed 114 sensors on the I-40 Bridge in Memphis, Tennessee, to fully characterize the response of the bridge to strong ground motion. The data acquisition system was upgraded in 2012, and it has been providing continuous real-time data. The data collection node was originally located at the AutoZone Headquarters building. Now it is at the Law School of the University of Memphis, located in downtown Memphis. Additional sensors were added to monitor the ground motion at the foundation level, located approximately 95 ft. below the bottom of the existing riverbed and about 130 ft. below the high-water level. Figure 2-1 shows the general location of the I-40 Bridge. Figure 2-2 shows a schematic of the main two-span tied-arch bridge indicating each sensor's general location and sensing direction. Similarly, Figure 2-3 shows the location and sensing direction of the sensors on the Arkansas-side approach spans.

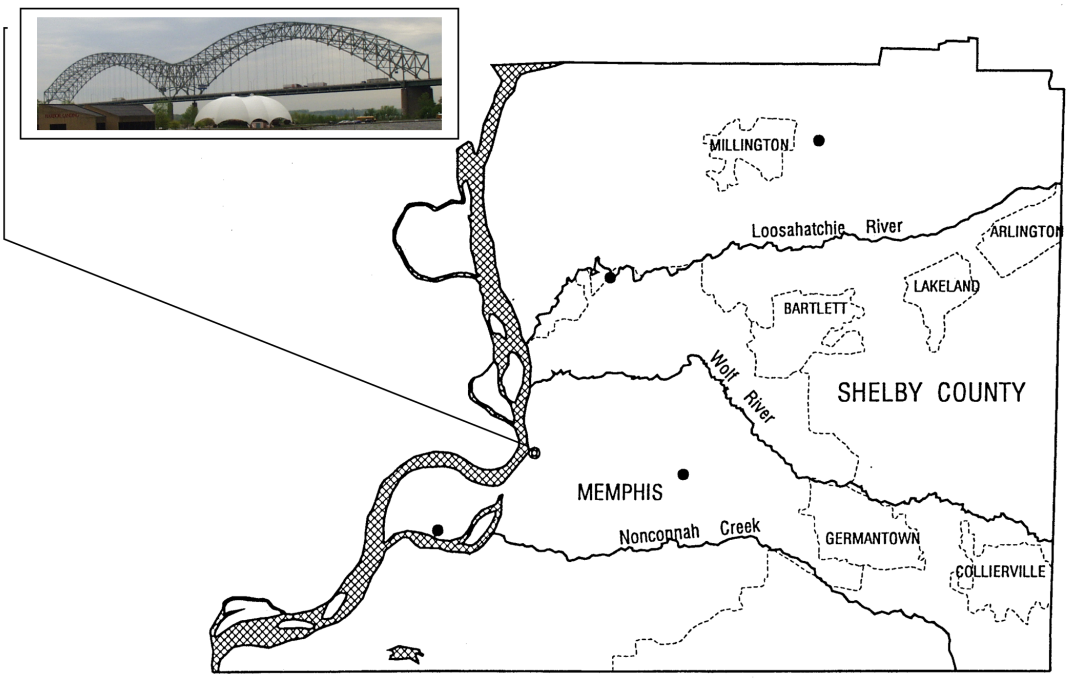


**Figure 2-1. Location of the I-40 Hernando de Soto Mississippi River Bridge.**

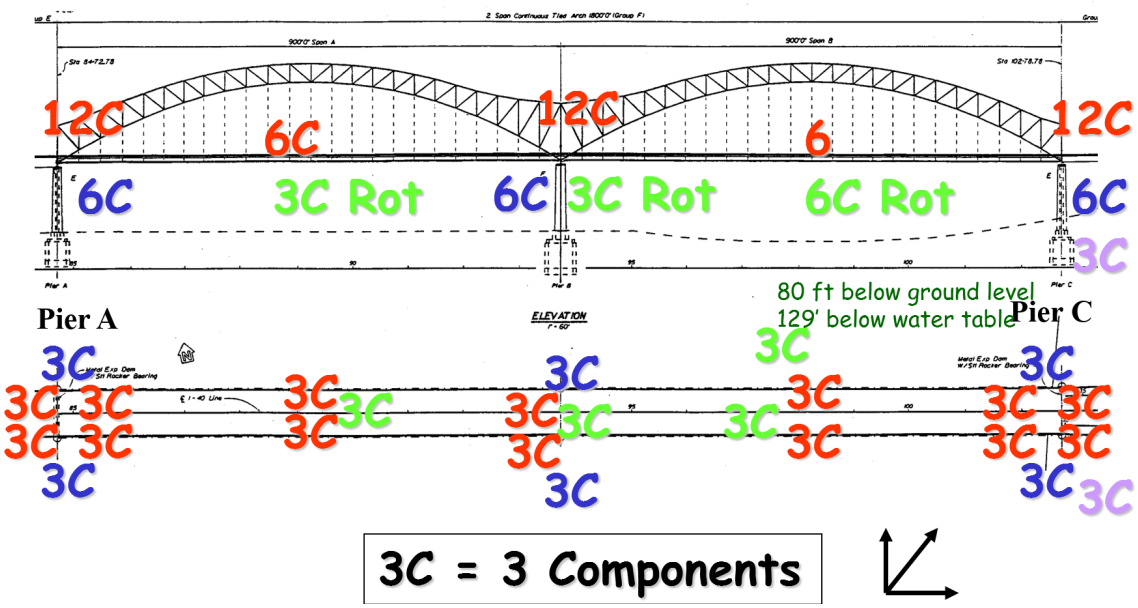


**Figure 2-2. Sensor locations on the main two-span tied-arch of the I-40 Bridge.**

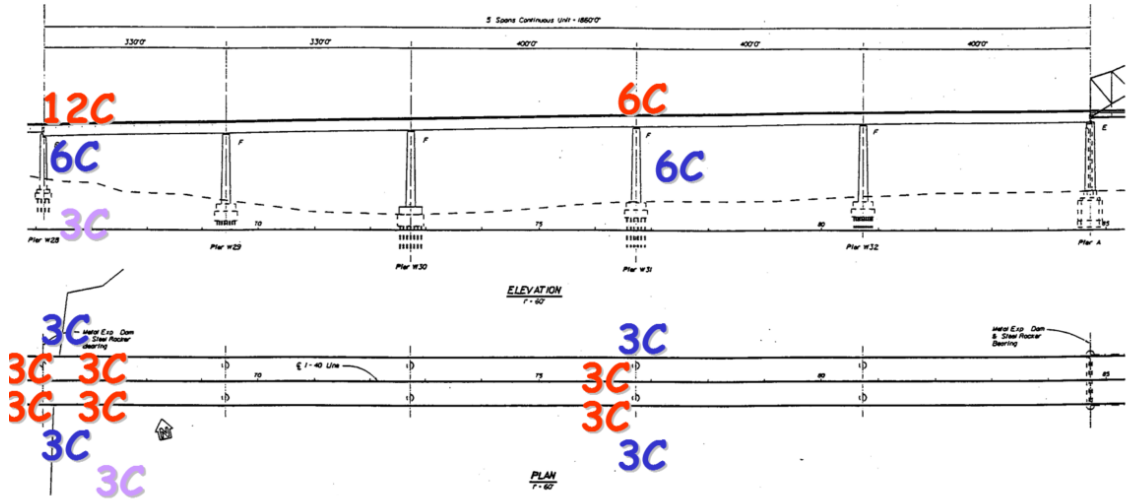


**Figure 2-3. Sensor locations on the west approach to the I-40 Bridge.**

The information to be measured from the sensors includes:

(1) free-field ground motion near the instrumented bridge,
(2) motion of the bridge foundation,
(3) site response,
(4) motion of the bridge below the isolation bearings,
(5) motion of the bridge above the isolation bearings,
(6) the spatial variation of ground motion along the total span; and
(7) lateral and torsional motion of the bridge.

In 2016, all the accelerometers on the bridge were replaced by triaxial Kinemetrics Episensors (with a full-scale range of ± 4G and broader bandwidth of 200 Hz). The Episensors used in the retrofit are the internal sensor deck version found in the Altus line of recorders. VLF Designs provided an interface card that contained a regulated power supply and transient protection and was fully compatible with the existing wiring infrastructure. Sensors were replaced using an adapter plate with mounting and leveling hardware that accommodated the new larger box that fitted existing clamps and sensor bases. All the equipment is housed in T304 stainless steel enclosures as specified by TDOT.

The east and west borehole sensors were replaced with 3-inch diameter shallow borehole Episensors. Bends in the existing 4-inch borehole pipes made it impossible to position the 4-inch diameter sensors from the original 2001 installation in the footings. The new sensor packages had no trouble negotiating the bends in the pipes. The borehole sensors are equipped with corrosion-proof yokes that allow loading poles to preset the orientation of the borehole Episensors. New splicing enclosures were installed on the pier caps adjacent to the boreholes, and the same interface card was used with the borehole sensors to provide protection and sensitivity normalization to the devices.

Isolated power converters on each card also help break any ground loops in the signal wiring and further protect components in the signal path from lightning-induced transients. Each interface card contains a calibration signal generator that provides an approximate ½G triangle wave capable of linearly exercising the mass and standard positive and negative pulses. The cal circuit is triggered by the basalt recorders, a switch in the sensor enclosure, or the 220MHz auxiliary command and control system. The buffer amps on these cards have a gain of 4 so that the full-scale sensor output is 40 Vp-p differentials. The gain of these amplifiers is made slightly variable so that during the initial sensor test and calibration, the sensors can be normalized to a gain of exactly 5V/G. There is also a provision for electronically removing slight offsets present at the accelerometer outputs after the cases have been leveled. A tightly regulated accelerometer and calibrator power supply also ensure that no noise or parameter shifts will occur when AC power is lost, and the system is running on slowly discharging batteries. Standard mode filtering on the power supply inputs ensures that no high frequency switching noise from the isolated power converter will cross-talk onto the signal wiring in the cable connecting the accelerometer to the recorder. The isolated power converters maintain a regulated output for DC input voltages between 9 and 18 VDC, thus encompassing all possible voltages to which the sensors may be exposed during normal operation.

# Chapter 3 Sensors Used in This Study

To monitor the behavior of the bridge and the change in its frequency signature after the crack occured, we focused on sensors near the the location of the crack. Figure 3-1 shows the general location of the crack and the sensors selected for this study. The sensors on Pier B are designated Node E, sensors on Pier C are Node G, and sensors at the mid-span are Node F. At each node, there are tri-axial sensors are located on both the north and south sides of the bridge. Each tri-axial sensor has one accelerometer in the longitudinal horizontal direction of the bridge (HN1), one in the transverse horizontal direction (HN2), and one in the vertical direction (HNZ). Tables 3-1 to 3-3 lists details on the locations of the sensors. The selected sensors are highlighted in Bold font in these tables. Table 3-4 lists the available saved data sets from these sensors from 2016 through 2021.

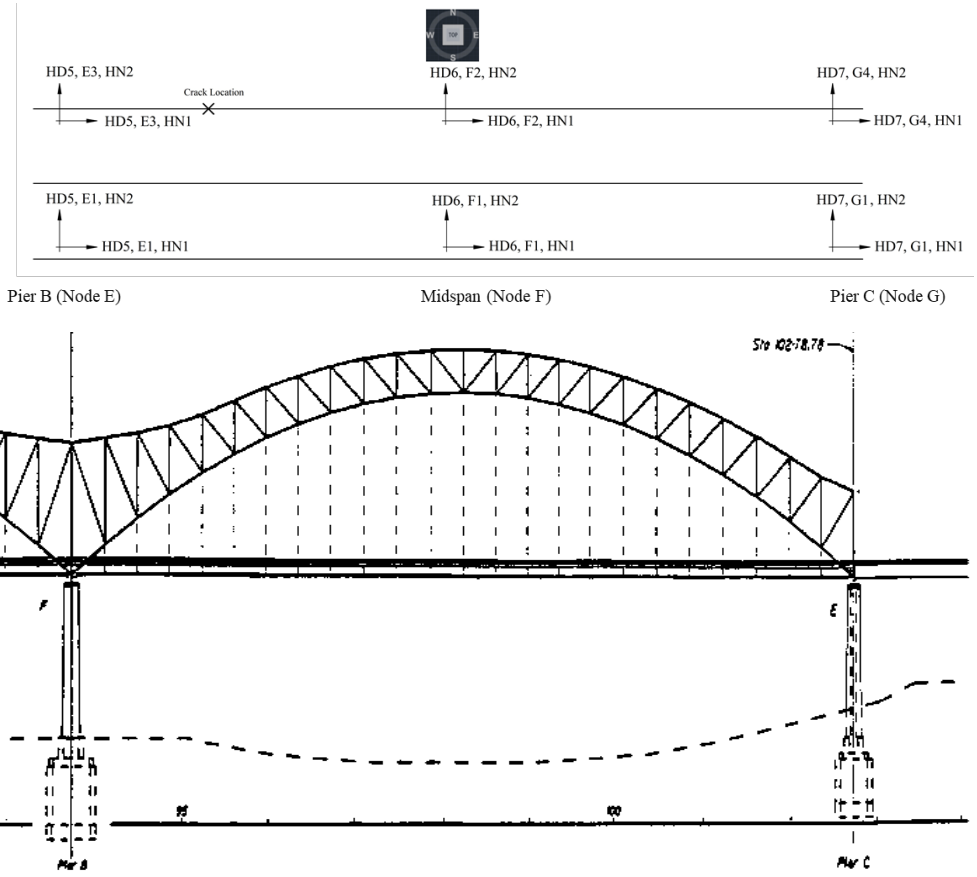


**Figure 3-1. Location and designation of sensors on the span of the I-40 Bridge with the cracked beam.**

**Table 3-1**
**Details on sensors placed on Pier B (Node E).**

| Channel | Location | Orientation | DAS number | DAS location | Sensor location |
|---|---|---|---|---|---|
| **HN1** | **E1** | **Longitudinal** | **HD5** | **Node E, Pier B, Main Span Midpoint** | **Midpoint Main Span, South** |
| **HN2** | **E1** | **Transverse** | **HD5** | **Node E, Pier B, Main Span Midpoint** | **Midpoint Main Span, South** |
| **HNZ** | **E1** | **Vertical** | **HD5** | **Node E, Pier B, Main Span Midpoint** | **Midpoint Main Span, South** |
| HN1 | E2 | Longitudinal | HD5 | Node E, Pier B, Main Span Midpoint | Pier B Cap, South |
| HN2 | E2 | Transverse | HD5 | Node E, Pier B, Main Span Midpoint | Pier B Cap, South |
| HNZ | E2 | Vertical | HD5 | Node E, Pier B, Main Span Midpoint | Pier B Cap, South |
| **HN1** | **E3** | **Longitudinal** | **HD5** | **Node E, Pier B, Main Span Midpoint** | **Midpoint Main Span, North** |
| **HN2** | **E3** | **Transverse** | **HD5** | **Node E, Pier B, Main Span Midpoint** | **Midpoint Main Span, North** |
| **HNZ** | **E3** | **Vertical** | **HD5** | **Node E, Pier B, Main Span Midpoint** | **Midpoint Main Span, North** |
| HN1 | E4 | Longitudinal | HD5 | Node E, Pier B, Main Span Midpoint | Pier B Cap, North |
| HN2 | E4 | Transverse | HD5 | Node E, Pier B, Main Span Midpoint | Pier B Cap, North |
| HNZ | E4 | Vertical | HD5 | Node E, Pier B, Main Span Midpoint | Pier B Cap, North |

**Table 3-2**
**Details on sensors placed on Midspan (Node F).**

| Channel | Location | Orientation | DAS number | DAS location | Sensor location |
|---|---|---|---|---|---|
| **HN1** | **F1** | **Longitudinal** | **HD6** | **Node F, Eastern Main Span B, Midpoint** | **Midpoint Main Span B, South** |
| **HN2** | **F1** | **Transverse** | **HD6** | **Node F, Eastern Main Span B, Midpoint** | **Midpoint Main Span B, South** |
| **HNZ** | **F1** | **Vertical** | **HD6** | **Node F, Eastern Main Span B, Midpoint** | **Midpoint Main Span B, South** |
| **HN1** | **F2** | **Longitudinal** | **HD6** | **Node F, Eastern Main Span B, Midpoint** | **Midpoint Main Span B, North** |
| **HN2** | **F2** | **Transverse** | **HD6** | **Node F, Eastern Main Span B, Midpoint** | **Midpoint Main Span B, North** |
| **HNZ** | **F2** | **Vertical** | **HD6** | **Node F, Eastern Main Span B, Midpoint** | **Midpoint Main Span B, North** |

**Table 3-3**
**Details on sensors placed on Pier C (Node G).**

| Channel | Location | Orientation | DAS number | DAS location | Sensor location |
|---|---|---|---|---|---|
| **HN1** | **G1** | **Longitudinal** | **HD7** | **Node G, Pier C, Eastern Terminus of Array** | **East End, Main Span B, South** |
| **HN2** | **G1** | **Transverse** | **HD7** | **Node G, Pier C, Eastern Terminus of Array** | **East End, Main Span B, South** |
| **HNZ** | **G1** | **Vertical** | **HD7** | **Node G, Pier C, Eastern Terminus of Array** | **East End, Main Span B, South** |
| HN1 | G2 | Longitudinal | HD7 | Node G, Pier C, Eastern Terminus of Array | West End, East Approach, South |
| HN2 | G2 | Transverse | HD7 | Node G, Pier C, Eastern Terminus of Array | West End, East Approach, South |
| HNZ | G2 | Vertical | HD7 | Node G, Pier C, Eastern Terminus of Array | West End, East Approach, South |
| HN1 | G3 | Longitudinal | HD7 | Node G, Pier C, Eastern Terminus of Array | Pier C Cap, South |
| HN2 | G3 | Transverse | HD7 | Node G, Pier C, Eastern Terminus of Array | Pier C Cap, South |
| HNZ | G3 | Vertical | HD7 | Node G, Pier C, Eastern Terminus of Array | Pier C Cap, South |
| HN1 | G4 | Longitudinal | HD7 | Node G, Pier C, Eastern Terminus of Array | East End, Main Span B, North |
| HN2 | G4 | Transverse | HD7 | Node G, Pier C, Eastern Terminus of Array | East End, Main Span B, North |
| HNZ | G4 | Vertical | HD7 | Node G, Pier C, Eastern Terminus of Array | East End, Main Span B, North |
| **HN1** | **G5** | **Longitudinal** | **HD7** | **Node G, Pier C, Eastern Terminus of Array** | **West End, East Approach, North** |
| **HN2** | **G5** | **Transverse** | **HD7** | **Node G, Pier C, Eastern Terminus of Array** | **West End, East Approach, North** |
| **HNZ** | **G5** | **Vertical** | **HD7** | **Node G, Pier C, Eastern Terminus of Array** | **West End, East Approach, North** |
| HN1 | G6 | Longitudinal | HD7 | Node G, Pier C, Eastern Terminus of Array | Pier C Cap, North |
| HN2 | G6 | Transverse | HD7 | Node G, Pier C, Eastern Terminus of Array | Pier C Cap, North |
| HNZ | G6 | Vertical | HD7 | Node G, Pier C, Eastern Terminus of Array | Pier C Cap, North |
| HN1 | G7 | Longitudinal | HD7 | Node G, Pier C, Eastern Terminus of Array | Borehole |
| HN2 | G7 | Transverse | HD7 | Node G, Pier C, Eastern Terminus of Array | Borehole |
| HNZ | G7 | Vertical | HD7 | Node G, Pier C, Eastern Terminus of Array | Borehole |

For every day in each month provided in Table 3-4, there are 96 records for the whole 24-hours of the day from 00:00 o'clock with an interval of 15 minutes. In this way, we processed the time-series data for every 15-minute time interval within a day, using the correction module of the SAC (Seismic Analysis Code) software. Then, a Fourier amplitude of the corrected data was evaluated for every recorded data. The data is cut off after the frequency of 100 Hz.

**TABLE 3-4**
**AVAILABLE RECORDED DATA FROM 2016 TO 2021.**

| Year / month | 2016 | 2017 | 2018 | 2019 | 2020 | 2021 |
|---|---|---|---|---|---|---|
| January | - | 27-29 | 20-22 | - | - | 3-5 |
| February | - | - | 23-25 | 5-7 | - | - |
| March | - | 15-17 | 26-28 | 7-9 | 1-3 | 19-21 |
| April | - | 14-16 | - | 6-8 | 2-4 | - |
| May | - | 12-14 | 3-5 | 11-13 | 7-9 | - |
| June | - | 12-14 | 4-6 | 11-13 | - | - |
| July | - | 13-15 | 5-7 | 13-15 | 3-5 | 12-31 |
| August | - | 13-15 | 6-8 | 12-14 | 15-17 | 1-14 |
| September | 17-19 | 14-16 | 29-30 | - | 18-20 | - |
| October | 17-19 | 14-16 | 1, 29-31 | 25-27 | 30-31 | - |
| November | 20-22 | 13-15 | 28-30 | - | 1 | - |
| December | 22-24 | 17-19 | 28-30 | 24-26 | - | - |

# Chapter 4 Results and Discussion

The data from 2016 to 2021 were analyzed to obtain the frequency content of the sensors at various locations on the I-40 Bridge. The distribution of frequencies can provide information on the fundamental behavior of the bridge. The data from the bridge follow the Standard for the Exchange of Earthquake Data (SEED) format and are collected in "miniSEED" or "m. SEED" formats. The SEED format, originally designed in the late 1980s, is widely used to archive and exchange seismological time series data and related metadata. The "miniSEED" file is the subset of the SEED standard that provides time-series data but does not include geographic coordinates, response/scaling information, and other interpreted information. Time series are independent data with fixed-length data records.

## *4.1 Signal Correction*

Analog or digital signals recorded from the sensors must be modified to obtain the correct ground motions. It is also important to measure the ground displacement, ground velocity, and ground acceleration and recover them from recorded signals. This is called correction for the instrument response.

In this project, SAC (Seismic Analysis Code) was used to correct all the recorded signals. SAC was originally developed at Lawrence Livermore National Laboratory to analyze data in time series. SAC processes waveforms and applied instrument corrections using poles and zeros files. Poles are the roots of the denominator of a transfer function, and zeros are the roots of the numerator of a transfer function. Generally, the number of poles is equal to or greater than the number of zeros.

All the needed files to process the signals are available on the Incorporated Research Institutions for Seismology (IRIS) website. All sensors installed on the I-40 Bridge have the same instrument correction zeros and poles. Figure 4-1 shows the zeros and poles used for the instrument correction used in this study.

```
* NETWORK   (KNETWK): NM
* STATION    (KSTNM): HDBR
* LOCATION   (KHOLE): G1
* CHANNEL   (KCMPNM): HN1
* CREATED           : 2021-09-22T01:59:23
* START             : 2016-09-01T00:00:00
* END               :
* DESCRIPTION       : The Hernando de Soto Bridge
* LATITUDE          : 35.153043
* LONGITUDE         : -90.058700
* ELEVATION         : 60.54
* DEPTH             : 0.0
* DIP               : 90.0
* AZIMUTH           : 90.0
* SAMPLE RATE       : 200.0
* INPUT UNIT        : M
* OUTPUT UNIT       : COUNTS
* INSTTYPE          :
* INSTGAIN          : 5.099000e-01 (M/S**2)
* COMMENT           :
* SENSITIVITY       : 2.142525e+05 (M/S**2)
* A0                : 2.459569e+13
* ********************************
ZEROS 2
+0.000000e+00 +0.000000e+00
+0.000000e+00 +0.000000e+00
POLES 4
-9.810000e+02 +1.009000e+03
-9.810000e+02 -1.009000e+03
-3.290000e+03 +1.263000e+03
-3.290000e+03 -1.263000e+03
CONSTANT      5.269688e+18
```

**Figure 4-1. Zero and poles used for the instrument correction.**

Figure 4-2 shows the signal collected by the sensor F1 in the horizontal direction (HN1) between 12:00 AM to 00:15 AM on September 17, 2016, before and after correction. The top panel of Figure 4-2 shows the uncorrected signal, and the bottom panel shows the corrected signal using poles and zeros. The corrected unit for the accelerations is $m/s^2$.

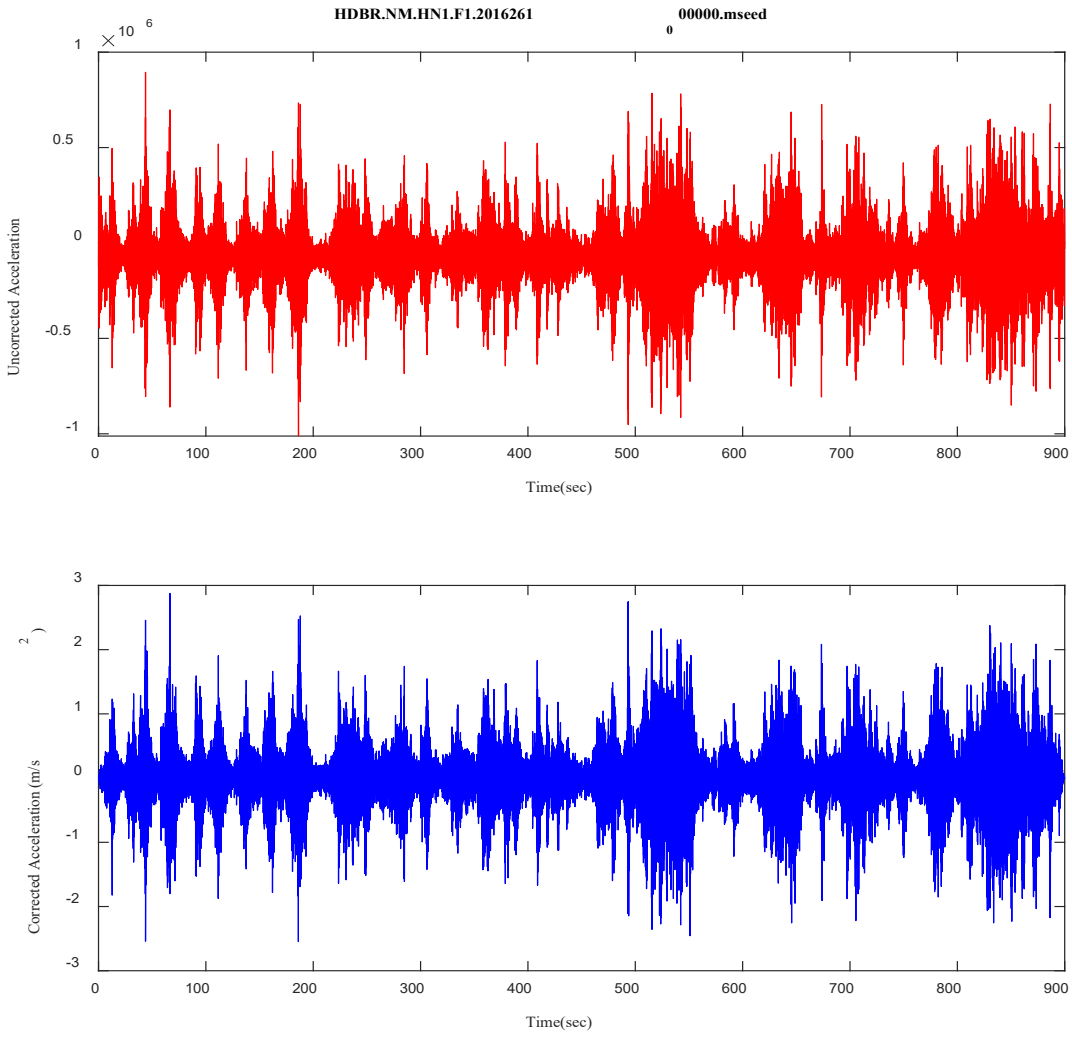


**Figure 4-2. Typical signal before and after correction.**

## *4.2 Fourier Amplitude Spectrum*

After signal correction, the data's discrete Fourier transform (DFT) was computed using a fast Fourier transform (FFT) algorithm. Fourier Amplitude Spectrum (FAS) contains the absolute value of the Fourier transform of the time series. The frequency range is defined by *n,* which determines the number of data points in the time series for the *n*-point DFT. The timestep of the time series is 0.005 seconds for all the signals. Each data set was recorded for 15 minutes or 900 seconds. Therefore, for a time step of 0.005 sec, there are 180,000 data points in each recorded signal. The FAS was computed for each 15 minute signal for all the data sets listed in Table 3-4. For example, Figure 4-3 shows the FAS between 12:00 AM and 00:15 AM, September 17, 2016, for sensor F1, channel HN1.

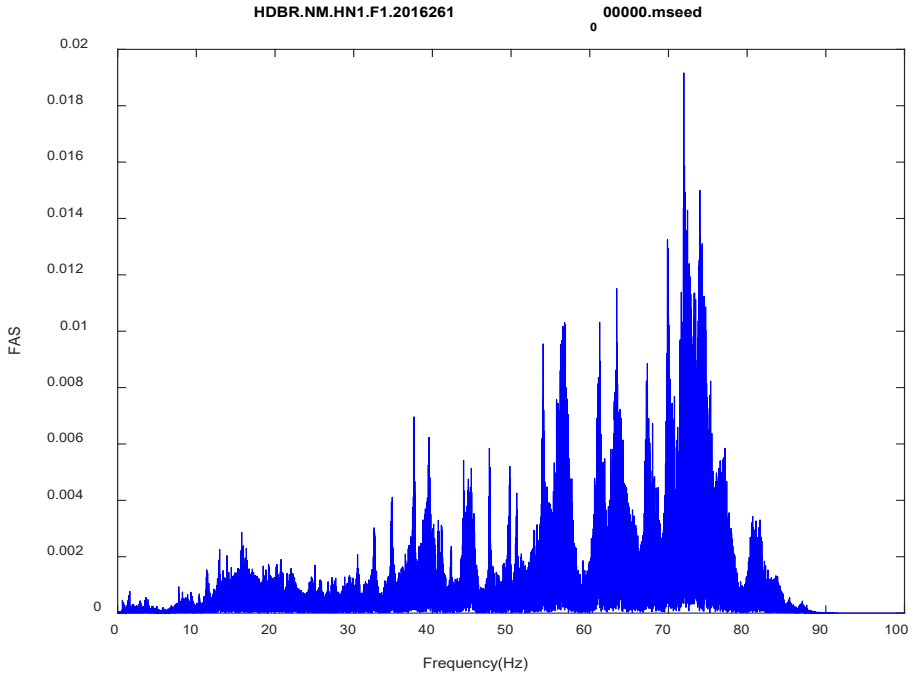


**Figure 4-3. Fourier Amplitude Spectrum (FAS) for channel HN1 of sensor F1 for 12:00 AM to 00:15 AM, September 17, 2016.**

## *4.3 Smoothing of the Fourier Amplitude Spectrum*

In most science experiments, the actual signal amplitudes (y-axis value) change smoothly as a function of x-axis values. In contrast, noise in the signal is a concern when recording ambient vibration in a structure, where the amplitude of the signal can change rapidly from point to point. A smoothing algorithm is applied to the data to reduce the noise. In general, data smoothing modifies the signal so that individual points that have a higher value than adjacent points are reduced, and the points that are lower increased. The true signal will not be distorted in this process, but high-frequency noise will be reduced. One of the most used smoothing algorithms is Savgol (Savitzky-Golay 1964) and is often used for preprocessing in signal processing. This algorithm can be used to reduce high-frequency noise in a signal. Figure 4-4 shows the smoothed Fourier amplitude spectrum for the data recorded between 12:00 AM and 00:15 AM, September 17, 2016, for sensor F1, channel HN1 using the Savgol algorithm.

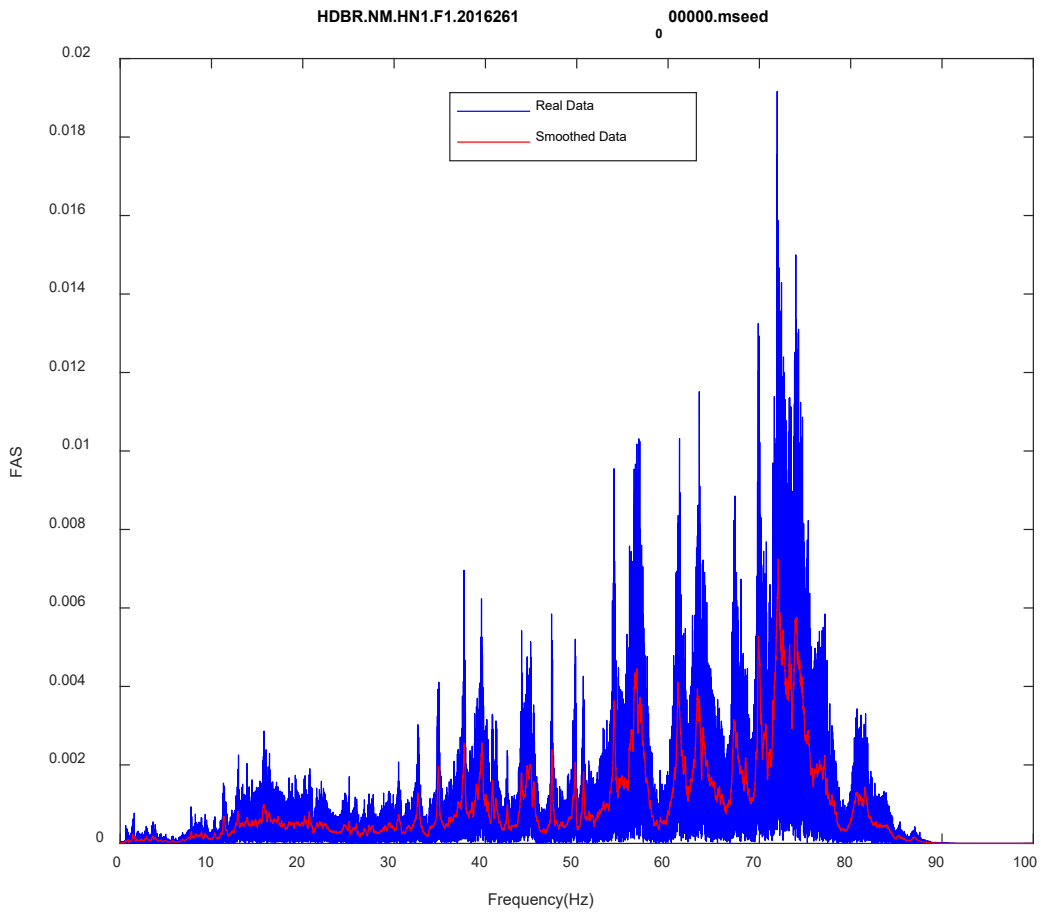


**Figure 4-4. The smoothed version of FAS versus real FAS for channel HN1 of sensor F1 for 12:00 AM to 00:15 AM, September 17, 2016.**

## *4.4 Correlation Between Smooth Data*

The correlation coefficient is a statistical measure of the strength of the relationship between the two variables. The correlation value ranges between -1.0 to 1.0, where -1 indicates a perfect negative correlation, while 1.0 is a perfect positive correlation. A correlation value of 0.0 shows no linear relationship between the two variables. In this study, the correlation between smoothed FAS data sets is utilized to identify changes in the frequency content of the recorded signals. The most common formula to calculate the correlation coefficient is the Pearson correlation coefficient *r*, which shows the linear dependency between the data sets. MATLAB is used to calculate the Pearson coefficient for all data sets. In MATLAB, the correlation coefficient $\rho(A,B)$ between two datasets, *A* and *B* with *N* scalar observations, is defined as:

$$\rho(A,B) = \frac{1}{N}\sum_{i=1}^{N}\left(\frac{A_i - \mu_A}{\sigma_A}\right)\left(\frac{A_i - \mu_B}{\sigma_B}\right) \qquad (3.1)$$

where $\mu_A$ and $\sigma_A$ are the mean and standard deviation of data set *A*, respectively, and $\mu_B$ and $\sigma_B$ are the mean and standard deviation of *B*.

The correlation coefficient matrix of two data sets is the matrix of correlation coefficients for each pairwise data set combination.

$$R = \begin{pmatrix} \rho(A,A) & \rho(A,B) \\ \rho(B,A) & \rho(B,B) \end{pmatrix} \tag{3.2}$$

Since *A* and *B* are always directly correlated to themselves, the diagonal entries are just 1, which yields the correlation coefficient matrix as below:

$$R = \begin{pmatrix} 1 & \rho(A,B) \\ \rho(A,B) & 1 \end{pmatrix} \tag{3.3}$$

The correlation coefficient matrix between the two smoothed FAS of the signals is computed for data sets listed in Table 3-4.

## *4.5 Bridge Data Analysis*

As listed in Table 3-4, there are a large number of data sets to evaluate. A selected subset of the recorded data was evaluated to reduce the size of the analysis and look for changes in the frequency content of the bridge, indicating changes in the bridge's structural signature. Data sets were selected based on the following criteria: (1) the same time of the year across all years to control for temperature and weather characteristics; and (2) data recorded on the same sensor in various years and 2021 before and after the retrofit. Data were recorded every year in August, except for 2016. For that year, data from September were included in the analysis.

Next, the correlation coefficients were computed for the August data at different times during the day to account for changes in temperature and traffic volume. Table 4-1 provides traffic count from 2010 at different times of the day.

**TABLE 4-1 TRAFFIC COUNT AT THE I-40 BRIDGE.**

| Time | Hourly Count |
|---|---|
| 00:00 - 01:00 | 865 |
| 01:00 - 02:00 | 657 |
| 02:00 - 03:00 | 517 |
| 03:00 - 04:00 | 547 |
| 04:00 - 05:00 | 767 |
| 05:00 - 06:00 | 1107 |
| 06:00 - 07:00 | 1863 |
| 07:00 - 08:00 | 2537 |
| 08:00 - 09:00 | 2559 |
| 09:00 - 10:00 | 2585 |
| 10:00 - 11:00 | 2655 |
| 11:00 - 12:00 | 2825 |
| 12:00 - 13:00 | 3040 |
| 13:00 - 14:00 | 3291 |
| 14:00 - 15:00 | 3171 |
| 15:00 - 16:00 | 3328 |
| 16:00 - 17:00 | 3302 |
| 17:00 - 18:00 | 2854 |
| 18:00 - 19:00 | 2527 |
| 19:00 - 20:00 | 2047 |
| 20:00 - 21:00 | 1855 |
| 21:00 - 22:00 | 1653 |
| 22:00 - 23:00 | 1325 |
| 23:00 - 24:00 | 1005 |

The correlation coefficients were computed for all sensors. As an example of the analysis, Figure 4-5 shows the correlation values for all directions of sensors F1 and F2 from September 17, 2016. The correlation matrices are presented in 15-minute segments for 24 hours. In Figure 4-5, the yellow color represents a prefect correlation of value 1. The time of day is indicated on both the horizontal and vertical axes in the correlation plots. In general, there are three common time intervals within the correlation matrix in yellow, indicating high correlations. Therefore, the day was divided into three regions that showed high correlations. These time intervals also corresponded to the various time intervals in the traffic count provided in Table 4-1.

Next, the best correlated data set in each of the time slots was selected based on the summation of the correlation coefficients in each row of the matrix. The summation value is used to indicate that a data set (recorded event) has the highest correlation with all other samples. Figure 4-6 shows the FAS, the corrected time-series signal, and the correlation metric for the three selected time intervals.

Following this strategy, three data sets were selected for each sensor. Figure 4-7 shows the correlation matrix for these three selected records and indicates that the correlation factors are close to 1 for sensors at Node F. These high correlation values suggest that the bridge's measured

frequency content is not affected by changes in traffic volume or temperature through the day. Similar results were obtained for all sensors at all nodes. Based on these results, the best-correlated data were used to represent each year.

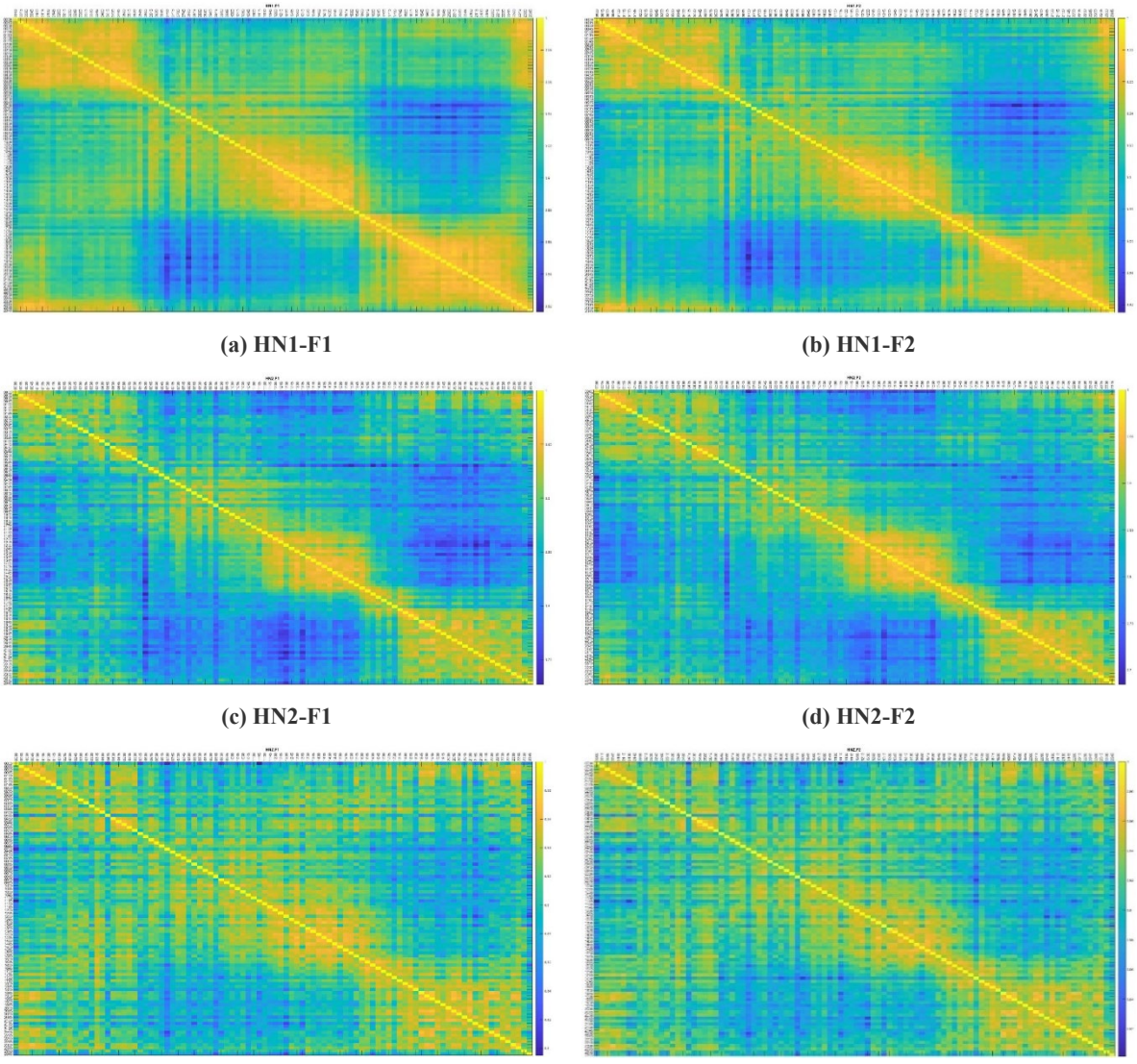

(a) HN1-F1 (b) HN1-F2

(c) HN2-F1 (d) HN2-F2

(e) HNZ-F1 (f) HNZ-F2

**Figure 4-5. Correlation matrix for Node F data from September 17, 2016.**

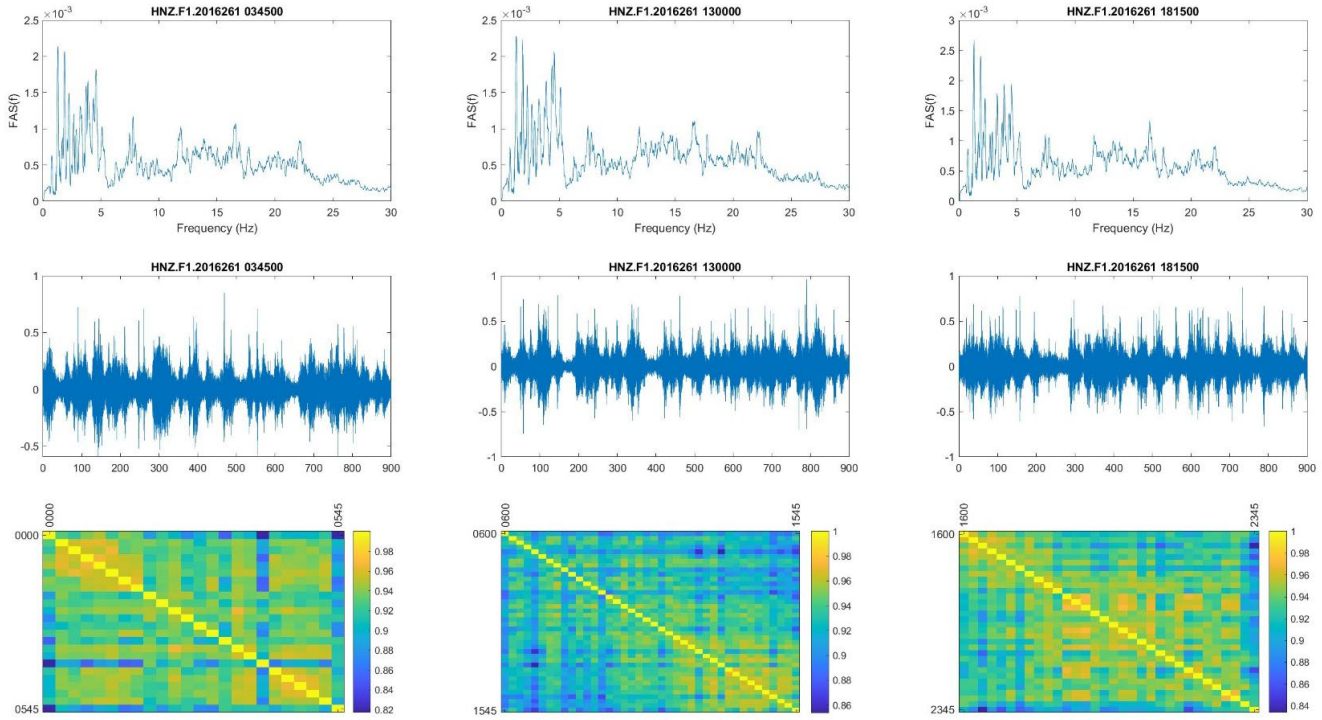


**(a) HNZ-F1**

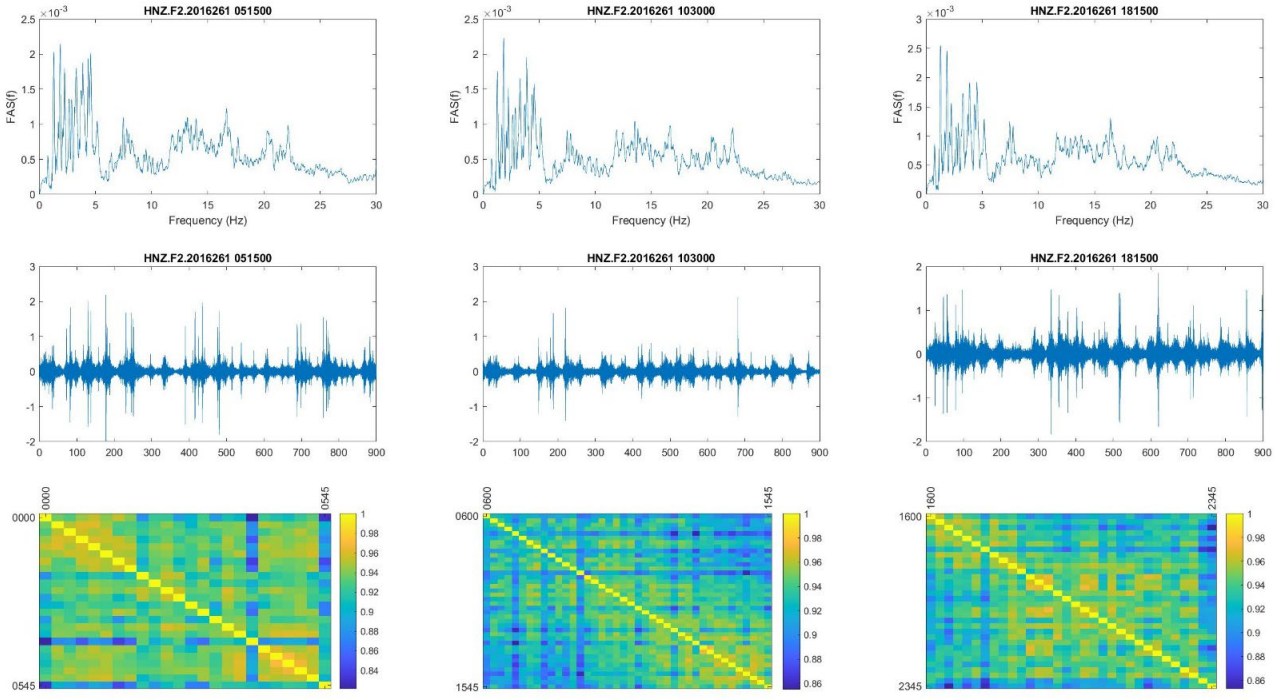


**(b) HNZ-F2**

**Figure 4-6. Correlation matrixes for Node F channel HNZ data at various times from September 17, 2016.**

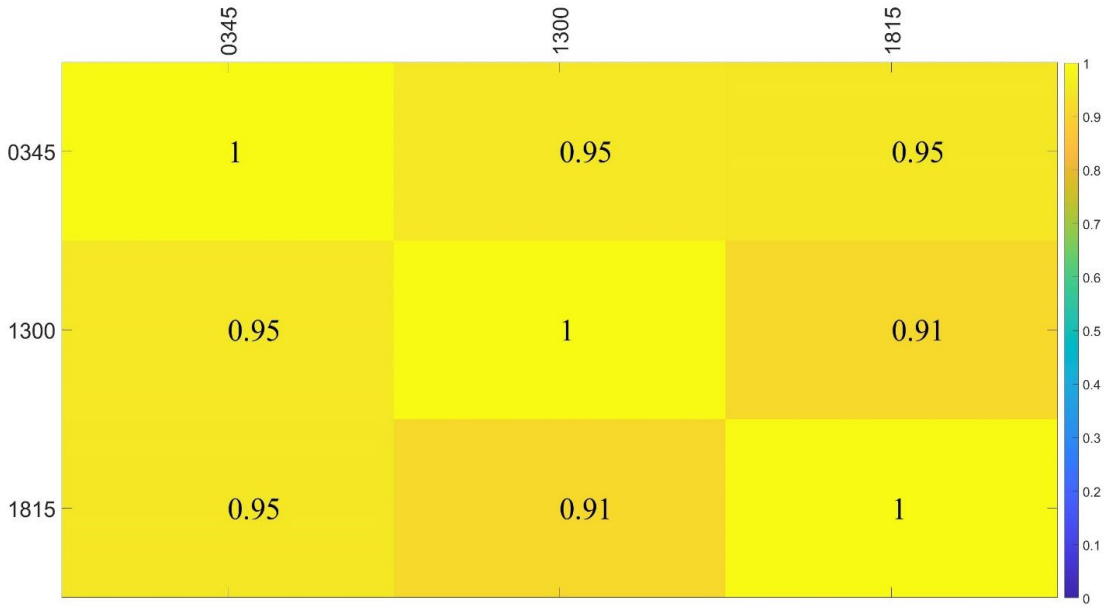


**(a) HNZ-F1**

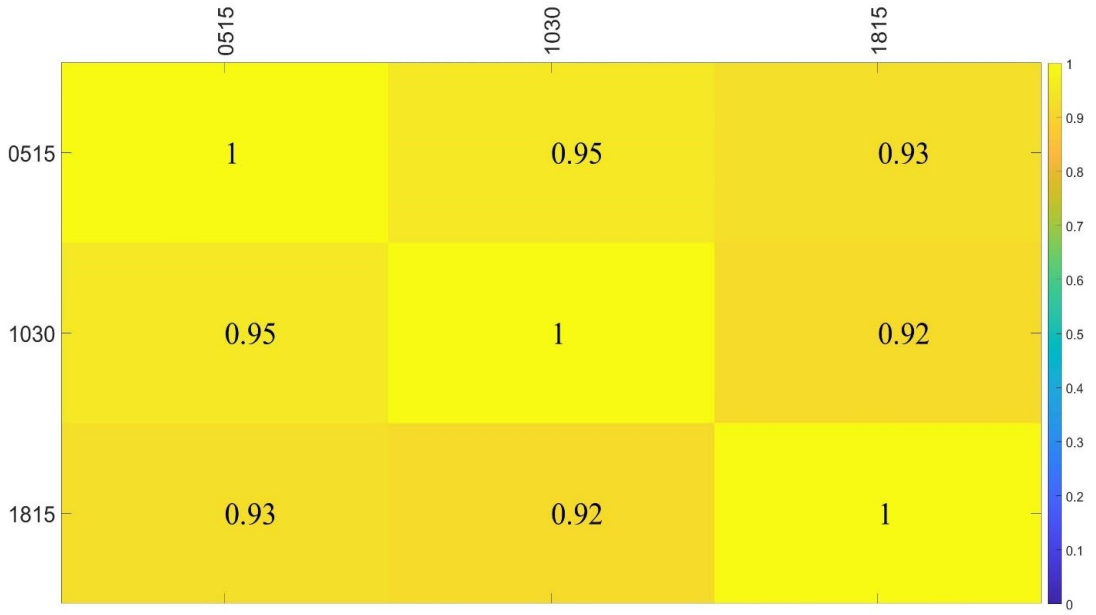


**(b) HNZ-F2**

**Figure 4-7. Correlation matrixes for the most correlated samples at Node F channel HNZ for each time interval from September 17, 2016.**

For the next part of the study, the best correlation data sets were compared from year to year. Also, four representative data sets from each year were used to improve the comparison. Each of the four daily data sets was selected as follows: (1) the most correlated sample over the day, (2) the most correlated sample in time interval 1, (3) the most correlated sample in time interval 2, and (4) the most correlated sample in time interval 3. Recall, the most correlated sample is the one that has the highest sum of correlation coefficients in a row of the matrix. Correlation matrixes were generated between the representative data sets for every sensor from 2016 to 2021.

Figures 4-8 to 4-11 show the Fourier spectrum, corrected time-series signal, and correlation matrices for the sensors mounted at the bridge mid-span (Node F) for the whole day time— HN1-F1, HN1-F2, HN2-F1, HN2-F2, HNZ-F1, and HNZ-F2, respectively. A comparison of Figures 4-8 to 4.11 for the sensors located at mid-span (Node F) indicates significant changes in correlation in 2018, decreasing dramatically in 2019 and 2020. It is worth noting that the correlation values go up again in 2021 after the retrofit, indicating similar behavior to that observed from 2016 and 2017. These results suggest that the structural behavior of the I-40 Bridge changes notably in 2018. The conclusion is that the change in the frequency content of the bridge suggests that the cracked beam began affecting bridge behavior in 2018 and continued throughout 2020.

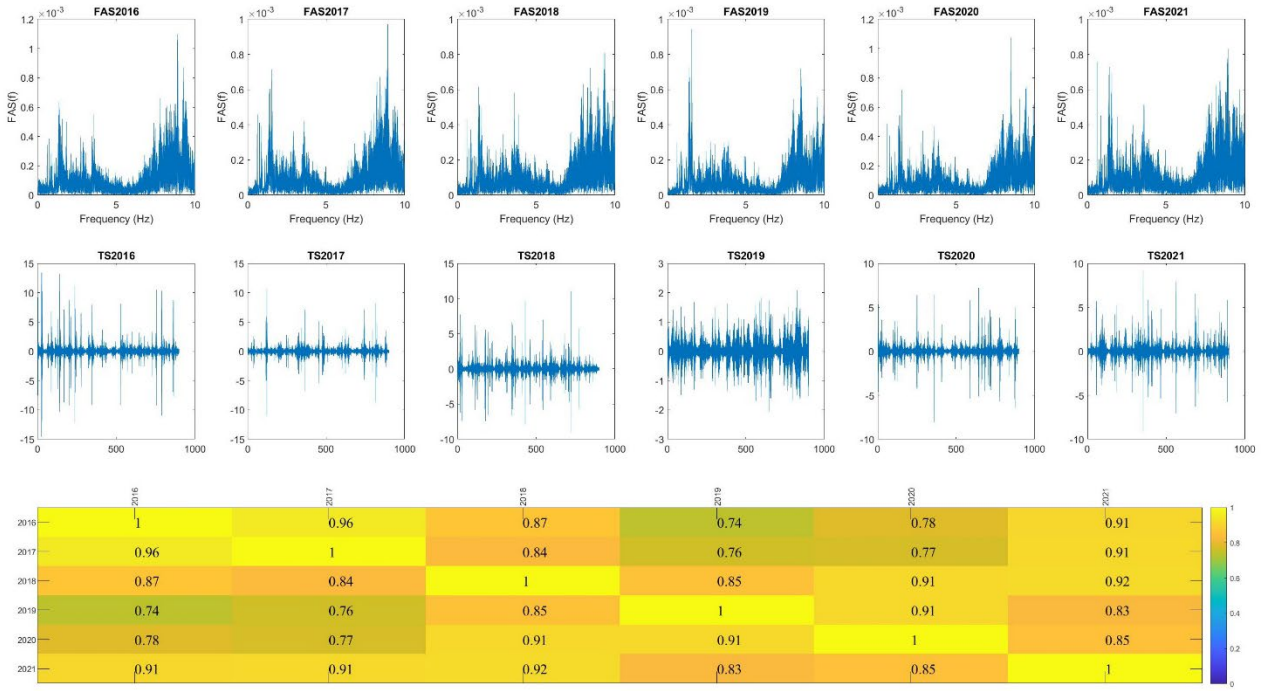


**Figure 4-8. Correlation matrixes for HN1-F1 from 2016 to 2021 for the whole day.**

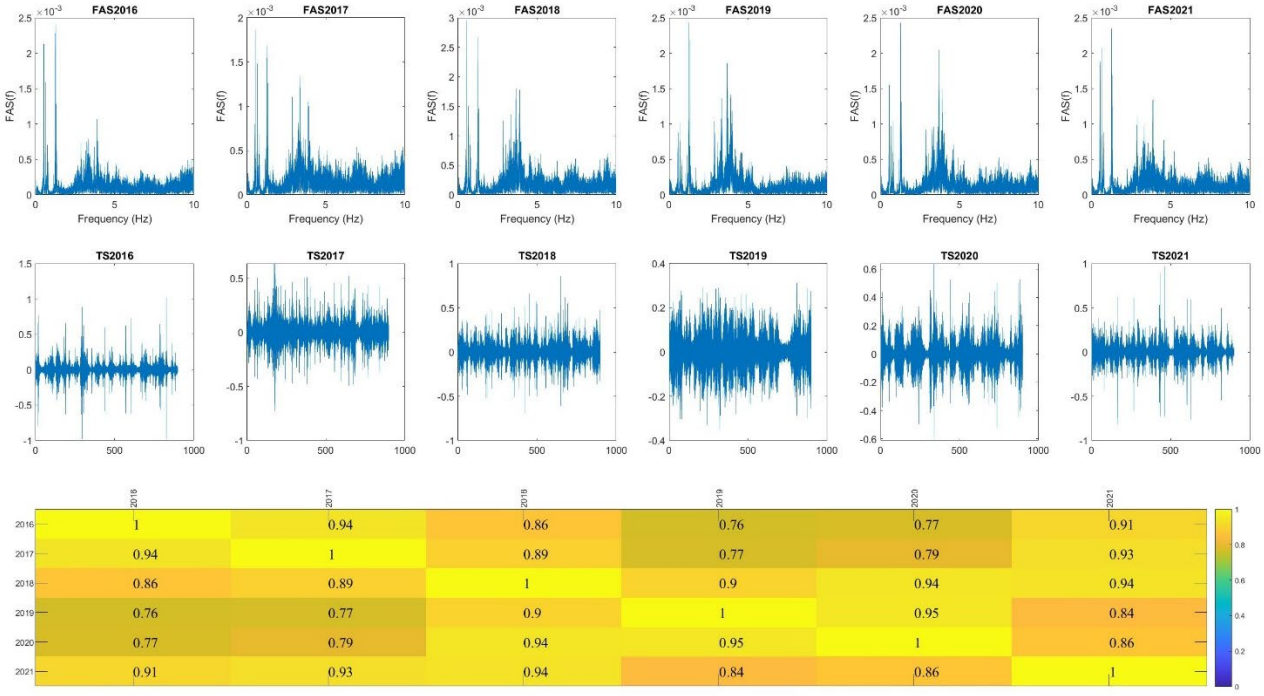


**Figure 4-9. Correlation matrixes for HN2-F2 from 2016 to 2021 for  the whole day.**

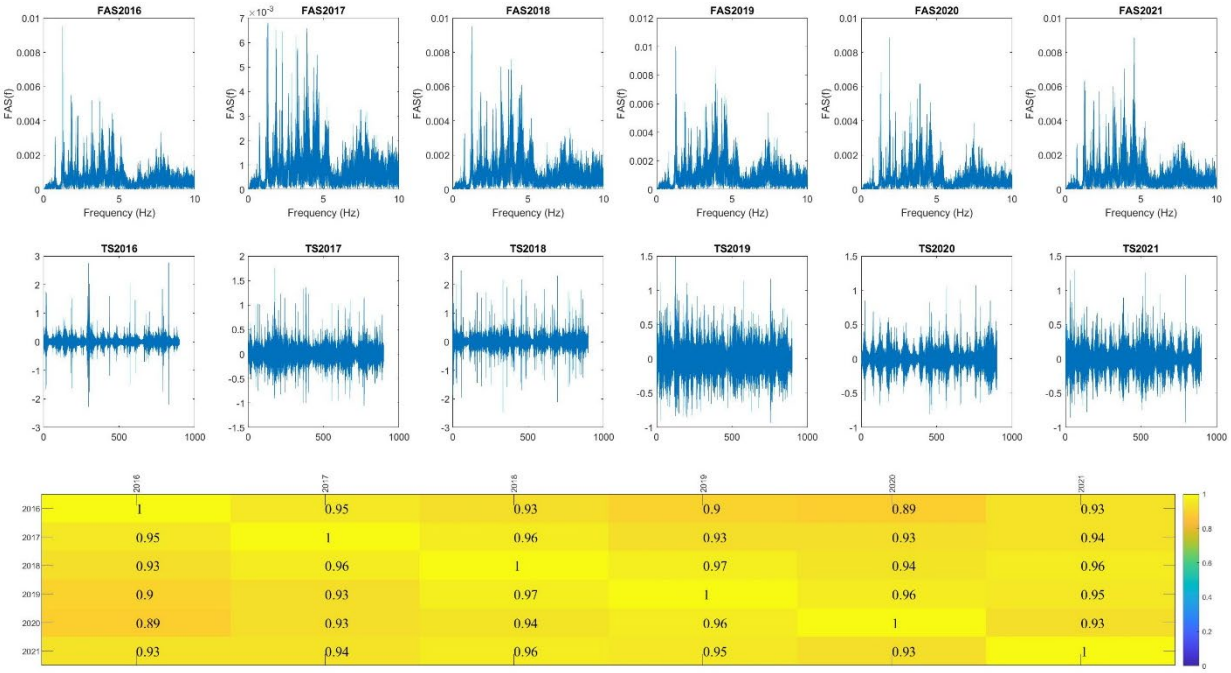


**Figure 4-10. Correlation matrixes for HNZ-F1 from 2016 to 2021 for the whole day.**

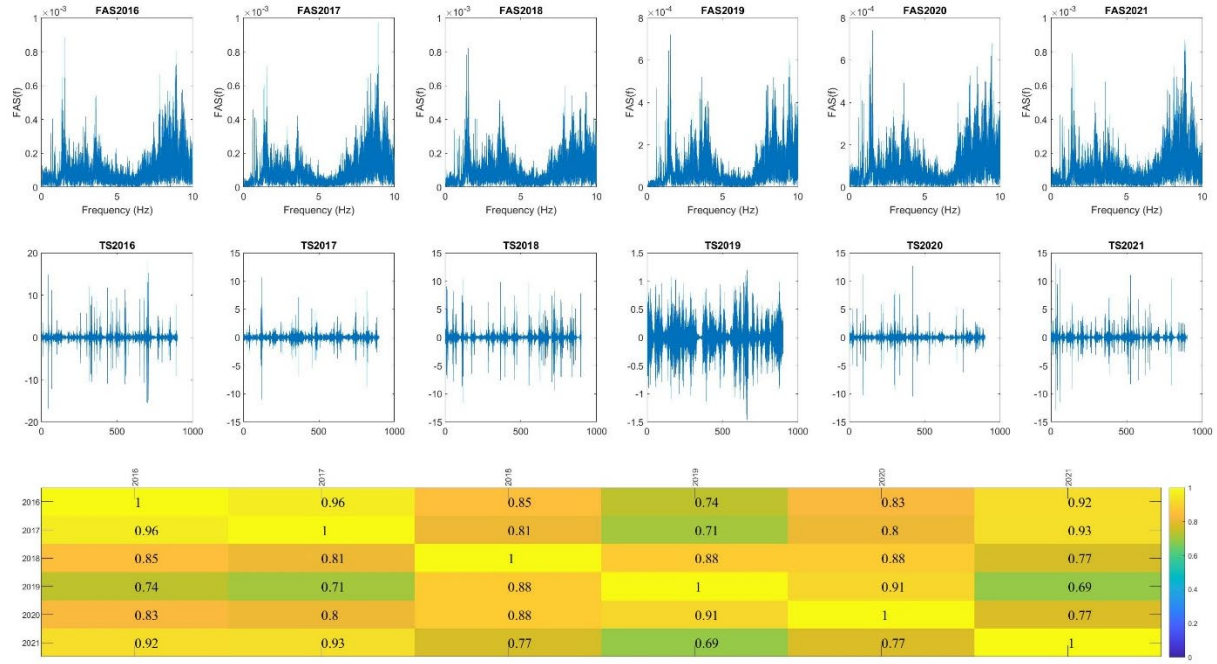


**Figure 4-11. Correlation matrixes for HN1-F2 from 2016 to 2021 for the whole day.**

# Chapter 5 Conclusion

The Hernando de Soto I-40 Bridge spans the Mississippi River and is part of I-40, a major east-west interstate highway running through the south-central portion of the United States. On May 11, 2021, the I-40 Bridge was closed after a crack in one of the major 900-ft horizontal beams was detected. Subsequence inspections conducted by officials from both the Tennessee and Arkansas departments of transportation revealed that the crack was there for several years. Despite much debate and many investigations, it was difficult to determine when the crack had first developed.

However, answering this question is critical because, in bridge designs like the I-40 Bridge, a crack in or the failure of critical elements might collapse the whole structure. Therefore, determining the time when the crack first affects the performance of the bridge and reviewing the actions within this period can be helpful to update and modify the strategies and regulations for health monitoring these structures.

In this research, an analysis of the data collected by a network of sensors on the I-40 Bridge installed and maintained by the University of Memphis was used to determine when the crack was initiated. Selected data sets were analyzed from 2016 to 2021 to obtain the frequency content of the bridge and determine any changes in its structural behavior. Based on the analysis, there was a notable change in the structural behavior of the bridge beginning in 2018 and continuing on through 2021.

The results indicate that the tension tie girder crack was first detected in the 2018 data and continued to develop in 2019 and 2020.

# References

Pezeshk, S., M. Withers, J. Bollwerk, R. McGoldrick, G. Steiner, and M. Yarnold, “Hernando de Soto I-40 Bridge Seismic Instrumentation Upgrade.” Contract No. RES2016-26, May 2018, Tennessee Department of Transportation Final Report.

Savitzky, A., and Golay, M.J.E., "Smoothing and Differentiation of Data by Simplified Least Squares Procedures," Anal. Chem. 1964, 36(8), 1627-1639. IRIS website http://ds.iris.edu/mda/NM/HDBR/